International Journal of Nanomedicine

Dovepress
open access to scientific and medical research

Open Access Full Text Article

ORIGINAL RESEARCH

Fabrication and Properties of a Biomimetic Dura Matter Substitute Based on Stereocomplex Poly (Lactic Acid) Nanofibers

This article was published in the following Dove Press journal:
International Journal of Nanomedicine

Di Chuan*
Yuelong Wang*
Rangrang Fan
Liangxue Zhou
Haifeng Chen
Jianguo Xu
Gang Guo

State Key Laboratory of Biotherapy and Cancer Center and Department of Neurosurgery, West China Hospital, Sichuan University, and Collaborative Innovation Center for Biotherapy, Chengdu 610041, People's Republic of China

*These authors contributed equally to this work

Background: Duraplasty is one of the most critical issues in neurosurgical procedures because the defect of dura matter will cause many complications. Electrospinning can mimic the 3D structure of the natural extracellular matrix whose structure is similar to that of dura matter. Poly(L-lactic acid) (PLLA) has been used to fabricate dura matter substitutes and showed compatibility to dural tissue. However, the mechanical properties of the PLLA substitute cannot match the mechanical properties of the human dura mater.

Methods and Results: We prepared stereocomplex nanofiber membranes based on enantiomeric poly(lactic acid) and poly(D-lactic acid)-grafted tetracalcium phosphate via electrospinning. X-ray diffraction results showed the formation of stereocomplex crystallites (SC) in the composite nanofiber membranes. Scanning electron microscope observation images showed that composites nanofibers with higher SC formation can keep its original morphologies after heat treatment, suggesting the heat resistance of composite nanofiber membranes. Differential scanning calorimeter tests confirmed that the melting temperature of composite nanofiber membranes was approximately 222°C, higher than that of PLLA. Tensile testing indicated that the ultimate tensile strength and the elongation break of the stereocomplex nanofiber membranes were close to human dura matter. In vitro cytotoxicity studies proved that the stereocomplex nanofiber membranes were non-toxic. The neuron-like differentiation of marrow stem cells on the stereocomplex nanofiber membranes indicated its neuron compatibility.

Conclusion: The stereocomplex nanofiber membranes have the potential to serve as a dura mater substitute.

Keywords: poly(lactic acid), dura matter substitute, stereocomplex crystallites, electrospinning

Introduction

One of the most critical issues in neurosurgical procedures is the closure of dura matter. Dura mater is the outermost and toughest layer of meninges. It is a connective tissue membrane that can protect the brain tissue.[1–3] Dura matter is also associated with the pathogenesis of some diseases.[4–6] It is composed of the cellular layer and the fibrous structure in which the fibers develop into multilayers and vary in orientations.[3] Meanwhile, dura matter is a fragile tissue that may be destroyed by trauma, brain surgery or tumor intrusion. The development of dura matter substitutes is a current focus of interest. Acellular swim bladder,[7] polymer membranes,[8–11] hydrogel,[12] and autologous fat[13] have been reported to be used in the repair of dura mater. However, polymer membranes and hydrogel are hard to

Correspondence: Gang Guo; Liangxue Zhou
State Key Laboratory of Biotherapy and Cancer Center, and Department of Neurosurgery, West China Hospital, Sichuan University, and Collaborative Innovation Center for Biotherapy, No. 17, Block 3, Southern Renmin Road, Chengdu 610041, People's Republic of China
Tel +86 28-8516 4063
Fax +86 28 85164060
Email guogang@scu.edu.cn; liangxue_zhou@126.com

submit your manuscript | www.dovepress.com
DovePress
http://doi.org/10.2147/IJN.S248998

mimic the physiological structure of the dura mater. And autologous transplantation will cause secondary damage.

Nanofibrous scaffolds hold great interest in tissue engineering. The design of scaffolds mimicking the structural and functional properties of the natural extracellular matrix (ECM) is a significant challenge.[14–17] Electrospinning is a fast and straightforward way to produce micro/nanofibers which can mimic the 3D structure of ECM whose structure is similar to that of the fibrous structure of dura matter.[18–21] The fibrous network of the electrospinning scaffold not only provides adhesion sites but also offers mechanical support to cells during the tissue repair process.[22–25] Therefore, electrospinning membranes seem to be a promising dura matter substitute.[3,26] Among the materials that have been reported to be used to fabricate electrospinning membranes for dura matter repair, it has been proved that poly(L-lactic acid) (PLLA) can reduce tissue adhesion and show compatibility to dural tissue.[10,27] Therefore, PLLA is a good choice to prepare the dura matter substitutes.

The mechanical properties of human dura matter have been investigated. The ultimate tensile strength of native human dura matter was tested as 7 ± 2 MPa.[28] At the same time, it also possesses a breaking strain of 116 ± 3% and good antiadhesion property.[12] It is really desired to prepare artificial dura matter substitutes with these properties for duraplasty. PLLA has been used to fabricate dura matter substitute and showed compatibility to dural tissue.[10,27] However, the mechanical properties of the PLLA substitute cannot match the properties of the human dura mater. The specific $CH_3\cdots O{=}C$ and $C_\alpha H\cdots O{=}C$ interactions between two stereoisomers of poly(lactic acid) (PLA) will lead to the formation of stereocomplex crystallites (SC).[29–31] Compared with pure PLLA membrane, membranes with SC formation exhibited enhanced mechanical and thermal properties.[32] Stereocomplex nanofibers prepared via electrospinning have drawn attention in recent years.[33,34] It has been proved that stereocomplex nanofibers are biocompatible in vivo.[35,36] Stereocomplex nanofiber membrane prepared by enantiomeric PLA may be a promising candidate for dura matter substitute.

Considering the intrinsic structural and mechanical properties of dura matter, this study prepared a stereocomplex nanofiber membrane as a candidate of artificial dura mater. The mechanical properties of the stereocomplex nanofiber membrane are close to that of dura matter. The maximal tensile strength and elongation break of the stereocomplex nanofiber membrane were 6.46 ± 0.07 MPa and 111.20 ± 4.7%, respectively. XRD proved the formation of SC in the stereocomplex nanofiber membrane. It was found that fibers with higher SC crystallinity can maintain its morphologies after heat treatment. Thermal properties of the stereocomplex nanofiber membrane were analyzed via differential scanning calorimeter (DSC). The melting temperature of the stereocomplex nanofiber membrane was around 222°C, higher than that of PLLA. In vitro cytotoxicity of nanofiber membranes and proliferation of bone marrow stem cells (MSCs) on nanofiber membranes were also investigated. The neuron-like differentiation of MSCs on the stereocomplex nanofiber membrane indicated its neuron system compatibility. These results can offer an innovative insight into the preparation of a biomimetic and neuron system compactable dura matter substitute.

Materials and Methods

Materials, Cells and Animals

PLA 4032D ($M_w = 2.1\times10^5$ g/mol, PDI = 1.7, 98% $_L$-isomer content) was obtained from NatureWorks. Tetracalcium phosphate (TTCP) was provided by Ensail Beijing Co., Ltd. (China). D-Lactide was purchased from Jinan Daigang Biomaterial Co., Ltd (China). Methylbenzene, dichloromethane (DCM) and petroleum ether were purchased from Chengdu Kelong Chemical Co., Ltd. (Chengdu, China). Stannous octanoate ($Sn(Oct)_2$), and 1,1,1,3,3,3-Hexafluoro-2-propanol (HFIP) were purchased from Aladdin Chemistry Co., Ltd (Shanghai, China). The mouse fibroblast cell (L929) was purchased from American Type Culture Collection (ATCC, USA.) Male Sprague-Dawley (SD) rats (1 week) were purchased from Chengdu Dossy Experimental Animals Co., Ltd (Chengdu, China). The Animal Ethics Committee of West China Hospital of Sichuan University granted permission for the experiments. All the animal procedures in the current study were performed in accordance with the Guidelines for Care and Use of Laboratory Animals of Sichuan University.

Preparation of Poly(D-Lactic Acid)-Grafted TTCP (g-TTCP)

TTCP was dried at 135°C for 12 h before use. TTCP was added into methylbenzene and dispersed under ultrasonication for 30 min. Then, the dispersed TTCP was added into the methylbenzene solution of D-lactide and reacted at 130°C for 12 h under nitrogen atmosphere. The reaction mixture was poured into cold petroleum ether. Precipitation was collected and dried in vacuum at 35°C to remove solvents. For grafting ratio analysis, the precipitation was extracted by DCM through

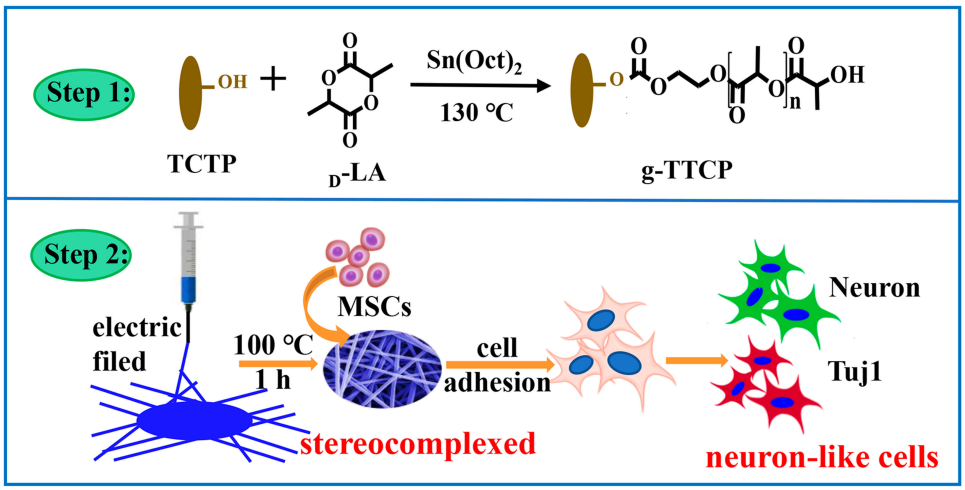

Schematic 1 The preparation process of stereocomplexed composite nanofibers.

a soxhlet extractor for 48 h and the product was recorded as g-TTCP. For electrospinning, the precipitation was extracted for 5 h and the product was recorded as g-TTCP-5.

Electrospinning

The electrospinning process was conducted as reported by our group.[37,38] g-TTCP-5 and PLA 4032D were added in HFIP/DCM (volume ratio of 5:1) with the final mass ratio of the mixture was 12% (w/v). The mixture was constantly stirred for 24 h before electrospinning. Nanofiber membranes with different mass ratios (g-TTCP-5/PLA 4032D = 0:1, 25:75, 35:65, 45:55, and 55:45) were recorded as PLA, PLA/TTCP25, PLA/TTCP35, PLA/TTCP45 and PLA/TTCP55. When electrospinning, feed rate of syringe pump was 1.0–2.0 mL/h. The voltage of FM-1206 electrospinning machine (Beijing Future Material Sci-tech Co., Ltd, China) was 18–20 kV. The distance between nozzle and collector was 15 cm. The total collection time for each sample was 4 h. To eliminate the residual solvent, the obtained nanofiber membranes were put into a vacuum oven at 35°C for 24 h.

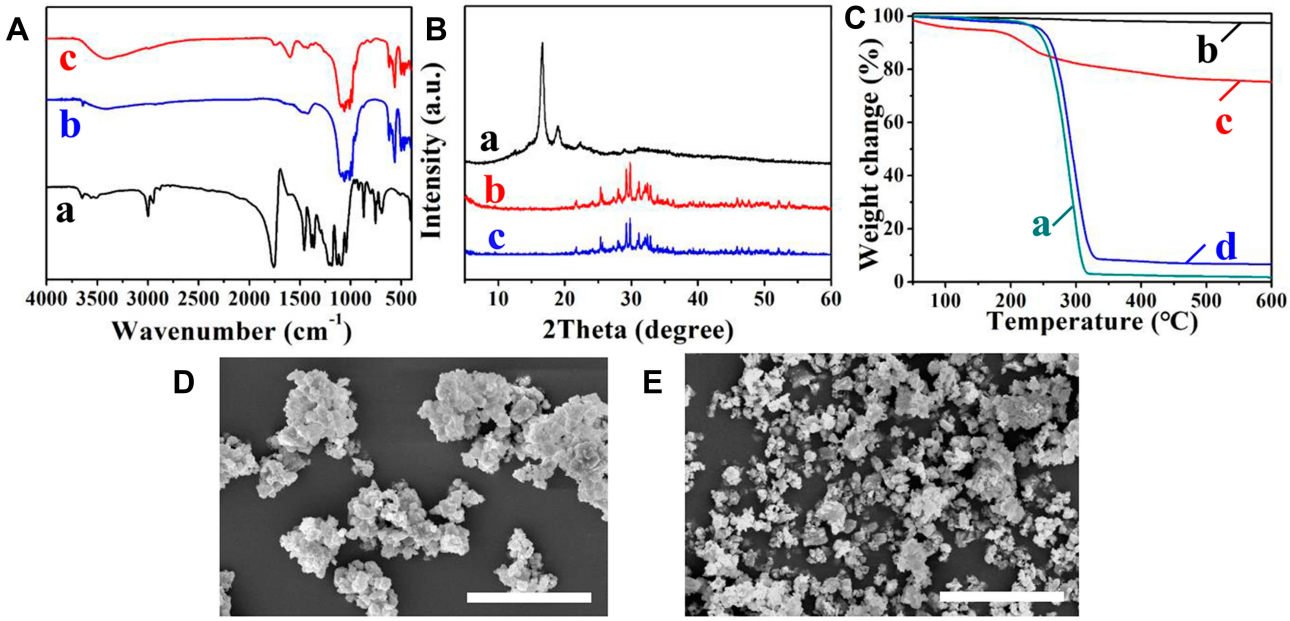

Figure 1 Characterization of DHA. (**A**) FT-IR spectra, (**B**) XRD curves and (**C**) TG analysis of (a) PDLA, (b) TTCP, (c) g-TTCP, and (d) g-TTCP-5. SEM image of (**D**) TTCP and (**E**) g-TTCP. Scale bars represent 20 μm.

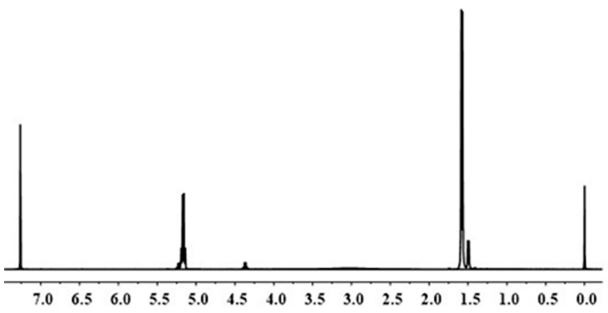

Figure 2 The ^{1}H-NMR spectroscopy of PDLA grafted on TTCP.

Fourier Transform Infrared (FT-IR) Spectroscopy

FT-IR spectra of PDLA, TTCP and g-TTCP were recorded by a Nicolet 6700 FT-IR spectrometer (Thermo Fisher Scientific, USA) in a wavenumber range of 4000–400 cm^{-1}.

X-Ray Diffraction (XRD)

XRD spectra were taken using Bruker D8 ADVANCE A25X (Bruker, Germany) equipped with Cu−Kα radiation (λ = 0.15406 nm) as X-ray source operating (40 kV, 40 mA) in the 2θ range of 5−60°. The crystallinity and fraction of SC in nanofibers were calculated by Jade 6.5 software according to the following equations:

$$X_{SC}(\%) = A_{SC}/(A_{SC} + A_{HC} + Aa) \times 100 \quad (1)$$

$$X_{HC}(\%) = A_{HC}/(A_{SC} + A_{HC} + Aa) \times 100 \quad (2)$$

$$f_{SC}(\%) = X_{SC}/(X_{SC} + X_{HC}) \times 100 \quad (3)$$

HC: homocrystallites. X_{SC}: crystallinity of SC, X_{HC} crystallinity of HC. A_{SC}: peak areas of SC, A_{HC}: peak areas of HC, Aa: peak areas of the amorphous phase, f_{SC}: the fraction of SC.

Differential Scanning Calorimeter (DSC)

The thermal behavior of nanofiber membranes was investigated using DSC (Q2000, TA Instruments, USA) under a nitrogen atmosphere. The temperature region was 20°C to 250°C. The heating rate was 10°C/min. The cooling rate was 5°C/min.

Thermalgravimetric (TG) Analysis

TG analysis was conducted under a nitrogen atmosphere with a heating rate of 10°C/min by TGA 550 (TA Instruments, USA). The temperature region was 30°C to 600°C.

Scanning Electron Microscope (SEM) Observation

Hitachi SU3500 SEM (Hitachi, Japan) was used to observe the morphologies of the nanofiber membranes. The diameters of around 100 fibers of each sample were recorded for diameter distribution analysis.

Transmission Electron Microscopy (TEM)

The dispersion of g-TTCP in nanofibers was observed by Hitachi H-600 TEM (Hitachi, Japan).

Mechanical Properties

Mechanical properties of nanofiber membranes were investigated by Instron 5976 (Instron, Norwood, MA, USA.) Membranes in this test were made into rectangles with a size of 10 × 65 mm. At least three samples of each group were tested. All samples were stretched until fractured. The thickness of the membranes tested was 100–160 μm.

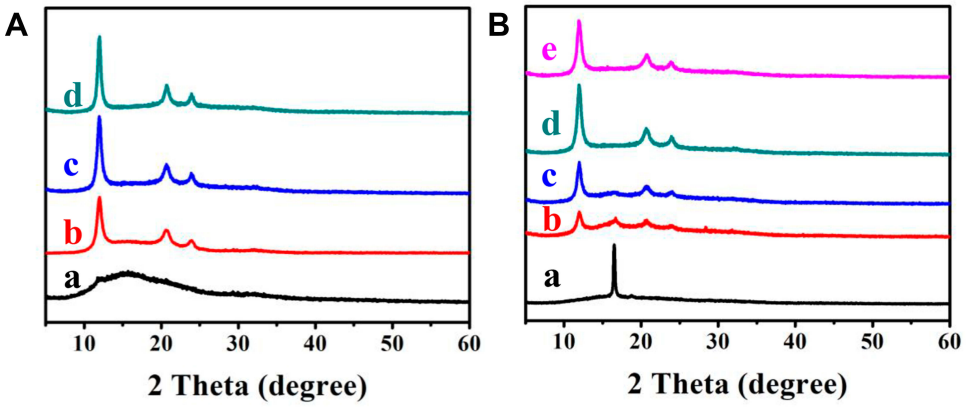

Figure 3 (**A**) XRD patterns of PLA/TTCP45 treated with different temperatures for 1 h. (a) 60°C; (b) 80°C; (c) 100°C; (d) 120°C; (**B**) XRD patterns of nanofiber membranes heated at 100°C for 1 h. (a) PLLA; (b) PLA/TTCP25; (c) PLA/TTCP35; (d) PLA/TTCP45; (e) PLA/TTCP55.

Table 1 The Crystallinity and Fraction of SC in Nanofiber Membranes

Sample	X_{SC} (%)	X_{HC} (%)	f_{SC} (%)
PLLA (100°C)	17.3		
PLA/TTCP25 (100°C)	17.5	4.9	78.1
PLA/TTCP 35(100°C)	29.8	0.8	97.4
PLA/TTCP45 (60°C)	–	–	–
PLA/TTCP 45 (80°C)	37.8	–	100
PLA/TTCP (100°C)	47.4	–	100
PLA/TTCP45 (120°C)	45.4	–	–
PLA/TTCP 55(100°C)	38.1	–	100

Abbreviations: X_{SC}, crystallinity of SC; X_{HC}, crystallinity of HC; f_{SC}, the fraction of SC.

Nuclear Magnetic Resonance Characterization (^{1}H-NMR)

To evaluate the number-average molecular weight of PDLA grafted on TTCP, g-TTCP was dispersed in deuterochloroform (CDCl3) to get the ^{1}H-NMR spectroscopy by Varian 400 spectrometer (Palo Alto, USA) at 400 MHz.

Biocompatibility Evaluation

The in vitro cytotoxicity of nanofiber membranes was investigated through Cell Counting Kit-8 (CCK-8) assay (Dalian Meilun Biotechnology Co., Ltd., China) in L929 cell line. Sterilized nanofiber membranes were incubated with High-Glucose Dulbecco's Minimum Essential Medium (H-DMEM, Hyclone, USA.) containing 10% fetal bovine serum (FBS, Gemini, USA) and 1% antibiotic (Solarbio, China) at 37°C for 2 days to prepare leaching solution of nanofiber membranes. L929 cells were seeded in 96-well plates with a density of 3×10^3 cells/well and cultured at 37°C for 24 h. Then, L929 cells in 96-well plates were cultured with the leaching solution for another 24 h. The cell viability was measured by CCK-8 assay. Bone marrow stromal stem cells (MSCs) were isolated from SD rats and the 4th passage was used.[39] The cell proliferation of MSCs seeded on stereocomplexed nanofiber membranes was measured by CCK-8 assay. MSCs were seeded in 96-well plates with a density of 5×10^3 cells/well and each well of the plate was covered by stereocomplex PLA/TTCP45. Low-Glucose Dulbecco's Minimum Essential Medium (L-DMEM, Hyclone, USA) containing 10% FBS were used to culture MSCs. After cultured for 1, 3, and 5 days, live/dead staining and SEM images of MSCs cultured on stereocomplexed PLA/TTCP45 were observed by fluorescent microscopy and Hitachi SU3500 SEM (Hitachi, Japan).

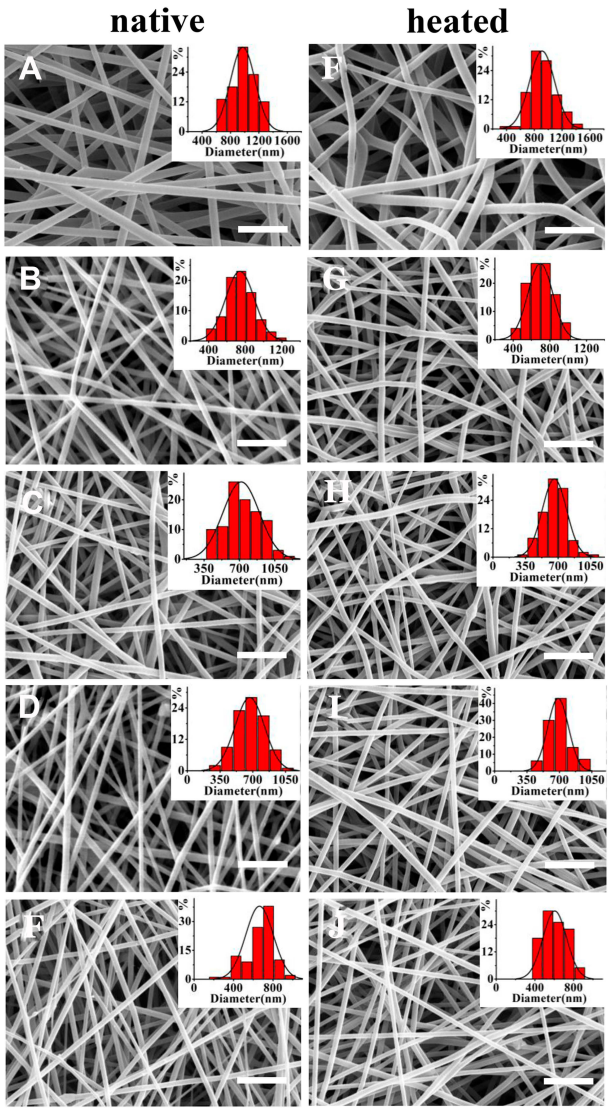

Figure 4 Morphologies of native (left) and heated (right) nanofiber membranes. (**A, F**) PLLA; (**B, G**) PLA/TTCP25; (**C, H**) PLA/TTCP35; (**D, I**) PLA/TTCP45; (**E, J**) PLA/TTCP55. Scale bar represents 4 μm.

Neuron-Like Differentiation of MSCs

MSCs were added into 24-well plates covered by glass, PLLA, and stereocomplexed PLA/TTCP45 and cultured with L-DMEM containing 10% FBS. The density of MSCs was 1×10^4 cells/well. After 24 h, the culture medium was replaced by L-DMEM containing 2% FBS and 10 ng/mL bFGF (MedChemExpress, USA). After 24 h, the medium was replaced by L-DMEM containing 2% FBS, 20 ng/mL bFGF and 20 ng/mL EGF (MedChemExpress, USA) every 3 days for 7 days. Then, cells were fixed with 2.5% glutaraldehyde and incubated in 0.1% Triton X-100 for 15 minutes. After that, cells were incubated with the primary antibody of Tuj1 (Cell Signaling Technology, USA.) and Neuron (Cell Signaling Technology, USA) overnight at 4°C and incubated

with secondary antibody (Abcam, UK) at 37°C for 1.5 h. Then, Apotome.2 (ZEISS, Germany) was used to take immunofluorescence images.

Results and Discussion

Characterization of g-TTCP

Schematic 1 showed the preparation process of g-TTCP. The FT-IR spectra of PDLA, TTCP, and g-TTCP are shown in Figure 1A. Compared with TTCP, g-TTCP had a new peak at 1767 cm^{-1} which was uniform with the peak of -C=O of PDLA, indicating the grafting of PDLA. The XRD curves of PDLA, TTCP, and g-TTCP are shown in Figure 1B. The peaks of g-TTCP at 2 theta angles of 25.41°, 29.32°, 29.84°, 32.41°, and 31.12° were the same as that of TTCP. No secondary phase was formed after the modification of PDLA. It indicated that g-TTCP maintained the intrinsic crystalline properties of TTCP.

TG analysis was used to study the grafting ratio of PDLA onto TTCP, and the results are shown in Figure 1C. Weight loss of TTCP, g-TTCP, g-TTCP-5 h and PDLA was 2.60%, 14.82%, 93.48%, and 98.35%, respectively. The grafting ratio of PDLA onto TTCP is calculated according to equation 1: Grafting ratio (%) =grafted PDLA on TTCP (g)/PDLA-grafted TTCP (g) × 100 (1). The PDLA grafted on TTCP of TTCP-PDLA was measured by TG analysis. The grafting ratio of PDLA on TTCP was 14.35%.

SEM images of TTCP and g-TTCP are shown in Figure 1D and E. The clusters of g-TTCP were smaller than that of TTCP. It suggested that g-TTCP may be more easily dispersed than TTCP.

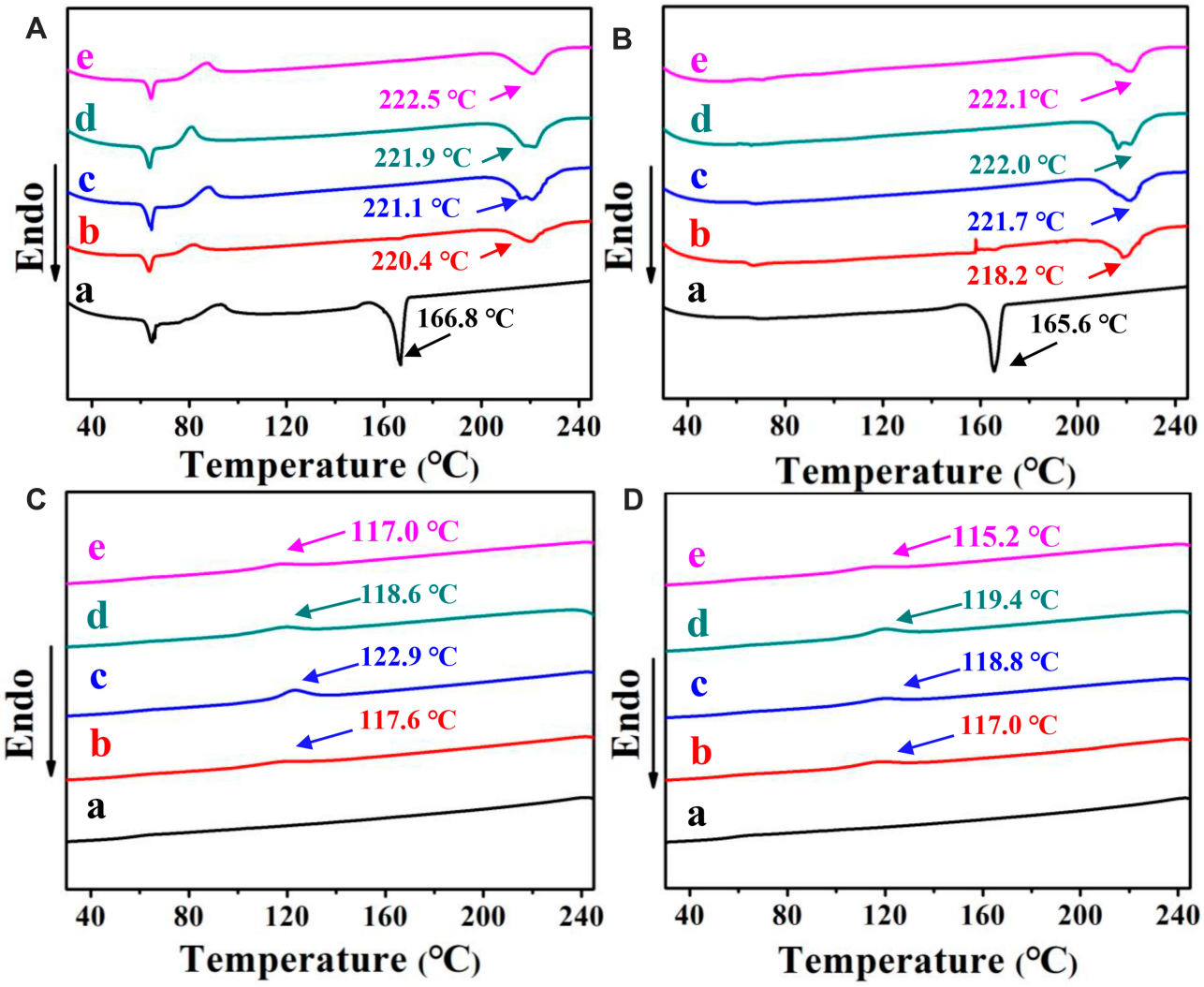

Figure 5 DSC thermogram of nanofiber membranes with different contents before (**A, C**) and after heating (**B, D**).

The ^{1}H-NMR spectroscopy of PDLA grafted on TTCP is shown in Figure 2. The methine peaks at 5.2 ppm (the middle methines) and 4.4 ppm (the terminal methines) can be observed. According to the peak areas of methine peaks, the number-average molecular weight of PDLA grafted on TTCP was around 2000.

SC Formation of Composite Nanofiber Membranes

In order to choose the proper temperature for heat treatment, native PLA/TTCP45 was heated at different temperatures for 1 h. The XRD results are exhibited in Figure 3 and Table 1. After heated at 60°C for 1 h, the curve of PLA/TTCP45 only had an amorphous phase. After heat treatment at higher temperatures, the peaks of SC can be observed at 11.8° (110), 20.6° (300/030), and 23.8° (220), which indicated the formation of SC (Figure 3A). The peaks of HC cannot be observed. The shearing force from the electric field led to the orientation of polymer chains, facilitating the SC formation in heated composite nanofibers.[40] The crystallinity and fraction of SC are shown in Table 1. It was found that the crystallinity of SC of nanofiber membrane heated at 100°C was 47.4%, higher than nanofiber membranes heated at 80°C (37.8%) and 120°C (44.36%). Therefore, nanofiber membranes were heated at 100°C for 1 h in the following studies.

The preparation process of stereocomplexed nanofibers was shown in Schematic 1. After treated at 100°C for 1 h, the SC formation of the membranes was tested by XRD and the results are shown in Figure 3B and Table 1. Heated PLA/TTCP45 and PLA/TTCP55 only had the peaks of SC at 11.8° (110), 20.6° (300/030), and 23.8° (220), while heated PLA/TTCP25 and PLA/TTCP35 had both peaks of SC and HC. The crystallinity and fraction of SC are shown in Table 1. It was found that the fraction of SC increased, while the fraction of HC decreased. The critical concentration of HC was much higher than that of SC. The growth of HC was suppressed resulting in the reduction of HC amount.[41,42]

Heat Resistance of Composite Nanofiber Membranes

SEM was used to observe the morphologies of nanofibers before and after heating (Figure 4). Diameter distributions of nanofibers of each group were presented in the histogram in Figure 4. The mean diameter of fibers of pure PLLA was around 1 μm. The mean diameters of composite nanofibers were between 600 and 770 nm. As shown in Figure 4, all nanofibers had a straight outlook before heat treatment. Fibers of PLA/TTCP45 and PLA/TTCP55 still maintained its straight outlook after heating. However, fibers of PLLA cannot maintain its straight outlook after heated at 100°C for 1 h. Some fibers of heated PLA/TTCP25 and heated PLA/TTCP35 were slightly bent as well. It indicated that fibers with higher SC crystallinity exhibited better heat resistance.

DSC was used to analyze the thermal activity of nanofiber membranes. The first DSC heating scans of nanofiber membranes were shown in Figures 4B and 5A. The relevant data are shown in Table 2. Pure PLLA membranes had one melting peak at around 166°C, which was the melting peak of HC. After adding g-TTCP-5, SC was generated in the membranes, as proved by the melting peak at around 221°C. SC was the dominant crystal phase in PLA/TTCP45 and PLA/TTCP55 because the melting peak of HC was hard to observe,[43] which was uniform with the results of XRD. Cooling sections of DSC were shown in Figures 4D and 5C. The cold crystallization peaks of pure PLLA were hard to observe while that of composite membranes emerged at around 118°C. It indicated that HC exhibited a lower crystallization rate than SC.[42,44]

Mechanical Properties of Nanofiber Membranes

The ultimate tensile strength and elongation at break of native human dura matter were tested as 7 ± 2 MPa and 116 ± 3%, respectively.[12,26] The typical stress–strain

Table 2 DSC Data of Nanofiber Membranes During the Heating Process

Sample	$^{SC}T_m$ (°C)	$\Delta^{SC}H_m$ (J/g)	$^{HC}T_m$ (°C)	$\Delta^{HC}H_m$ (J/g)
PLLA	–	–	166.8	45.8
PLLA (100 °C)	–	–	165.6	42.8
scPLA/TTCP25	220.5	34.7	166.8	1.0
scPLA/TTCP25 (100°C)	218.2	35.8	166.2	1.1
scPLA/TTCP35	221.1	43.9	–	–
scPLA/TTCP35 (100°C)	221.7	44.7	–	–
scPLA/TTCP45	221.9	45.8	–	–
scPLA/TTCP45 (100°C)	222.0	46.3	–	–
scPLA/TTCP55	222.5	42.4	–	–
scPLA/TTCP55 (100°C)	222.1	44.7		–

Abbreviations: $^{SC}T_m$, melting temperature SC; $^{HC}T_m$, melting temperature of HC; ΔH_m, crystallization enthalpy change.

curves of each group are shown in Figure 6A and B. The tensile strength and elongation break of each group are shown in Figure 6C and D. After the addition of g-TTCP-5, the ultimate tensile strength of native nanofiber membranes exhibited a decreasing trend. After heated at 100°C for 1 h, the ultimate tensile strength of all composite membranes was increased, especially that of PLA/TTCP25 (6.19 MPa), PLA/TTCP35 (6.35 MPa), and PLLA/TTCP 45 (6.46 MPa) which increased by 28.42%, 38.60%, and 27.41%, respectively, comparing with the corresponding native nanofiber membranes. The elongation break of composite nanofiber membranes decreased compared with that of PLLA fibers. The elongation break of heated PLA/TTCP25, PLA/TTCP35, PLA/TTCP45, and PLA/TTCP55 was 122.43%, 119.01%, 111.20%, and 93.73%, respectively. The ultimate tensile strength and elongation at break of native human dura matter were tested as 7 ± 2 MPa and 116 ± 3%, respectively.[12,26] The mechanical properties of the composite nanofiber membranes were close to that of native human dura matter, especially PLA/TTCP45. The TEM image of PLA/TCP45 is shown in Figure 6E. It can be observed that monodisperse TTCP particles were arranged one by one in the nanofiber of PLA/TCP45. The decrease of the tensile strength of PLA/TTCP55 should owe to the increased content of g-TTCP because the blocking effect of TTCP made the risk of destroying by outside force increase.[45,46]

In vitro Biocompatibility

In order to evaluate the in vitro cytotoxicity of nanofiber membranes, the leaching solution of each group was used to culture L929 cells for 24 h. The results of the cell viability of each group measured by CCK-8 assay are shown in Figure 7D. The group cultured on glass was set as the control. Compared with control, the cell viability of nanofiber groups was not suppressed, indicating the non-toxicity

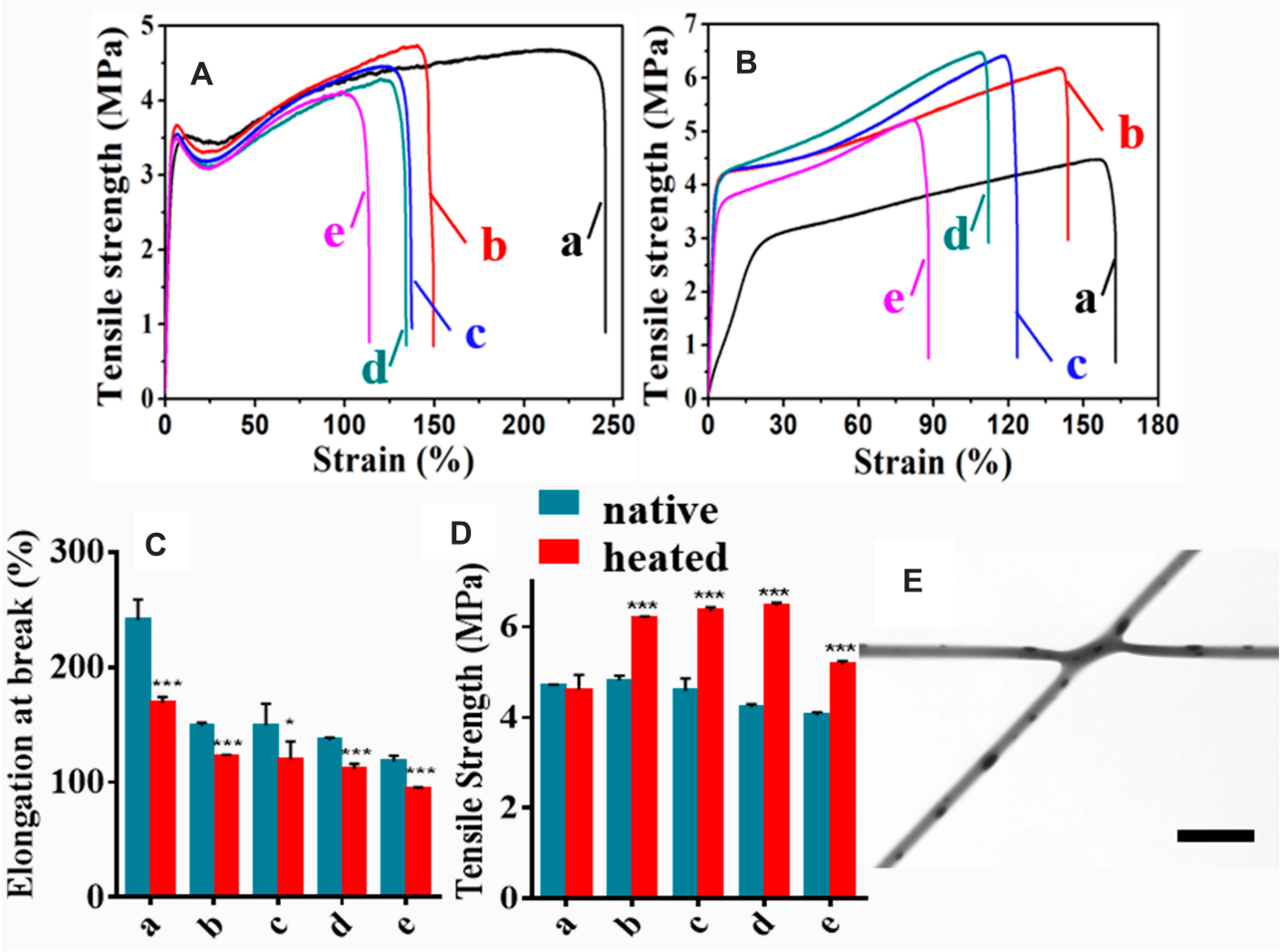

Figure 6 Mechanical properties of nanofiber membranes. Typical stress curves of (**A**) native and (**B**) heated nanofiber membranes. (**C**) Elongation break and (**D**) tensile strength of nanofiber membranes. (a) PLLA; (b) PLA/TTCP25; (c) PLA/TTCP35; (d) PLA/TTCP45; (d) PLA/TTCP55. (**E**) The TEM image of PLA/TTCP45. Scale bar represents 4 μm. *P<0.5, ***P<0.01.

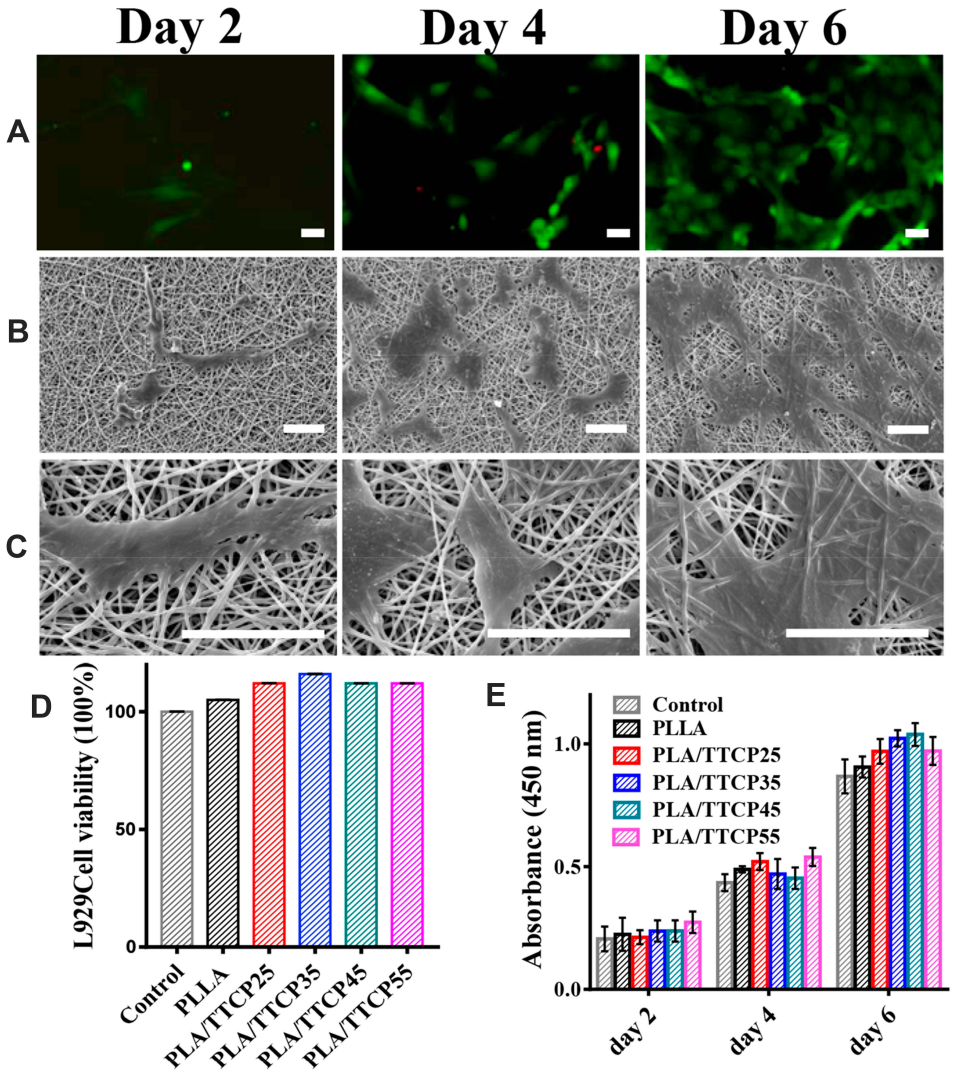

Figure 7 (**A**) Live/Dead staining of MSCs seeded on scPLA/TTCP45. SEM images of MSCs cultured on scPLA/TTCP45 with 500× magnification (**B**) and 2000× magnification (**C**). Scale bars represent 30 μm. (**D**) In vitro cytotoxicity assay of nanofiber membranes measured by CCK-8 assay. (**E**) MSCs proliferation on nanofiber membranes measured by CCK-8 assay.

of nanofiber membranes. The proliferation of MSCs was tested by CCK-8 assay and results are shown in Figure 7E. It can be seen that MSCs cultured on nanofiber membranes exhibited time-dependent proliferation, suggesting biocompatibility of nanofiber membranes.

In consideration of the crystallinity of SC and the mechanical properties of composites membranes, we chose PLA/TTCP45 to study the adhesion and proliferation of MSCs. Figure 7A–C showed the live/dead staining and SEM images of MSCs cultured on PLA/TTCP45 for 2, 4, and 6 days. It can be observed that dead cell (red) was hardly found at day 6 and the number of MSCs exhibited time-depended increase. The pseudopodia of MSCs observed by SEM proving the excellent adhesion of MSCs on PLA/TTCP45.

Neuron-Like Differentiation of MSCs

The expression of tuj1 and neuron of MSCs seeded on nanofiber membranes was observed by immunofluorescence imaging (Figure 8). After differentiation for 9 days, all three groups exhibited the expression of tuj1 and neuron. It suggested that MSCs could differentiate into neuron-like cells on PLA/TTCP45 as on PLLA and glass, indicating the neuron compatibility of PLA/TTCP45.

Conclusion

Stereocomplexed composite nanofiber membranes based on PLA and PDLA-grafted TTCP were prepared via electrospinning. After heated at 100°C for 1 h, SC formed in composite nanofibers. The crystallinity of SC of PLA/

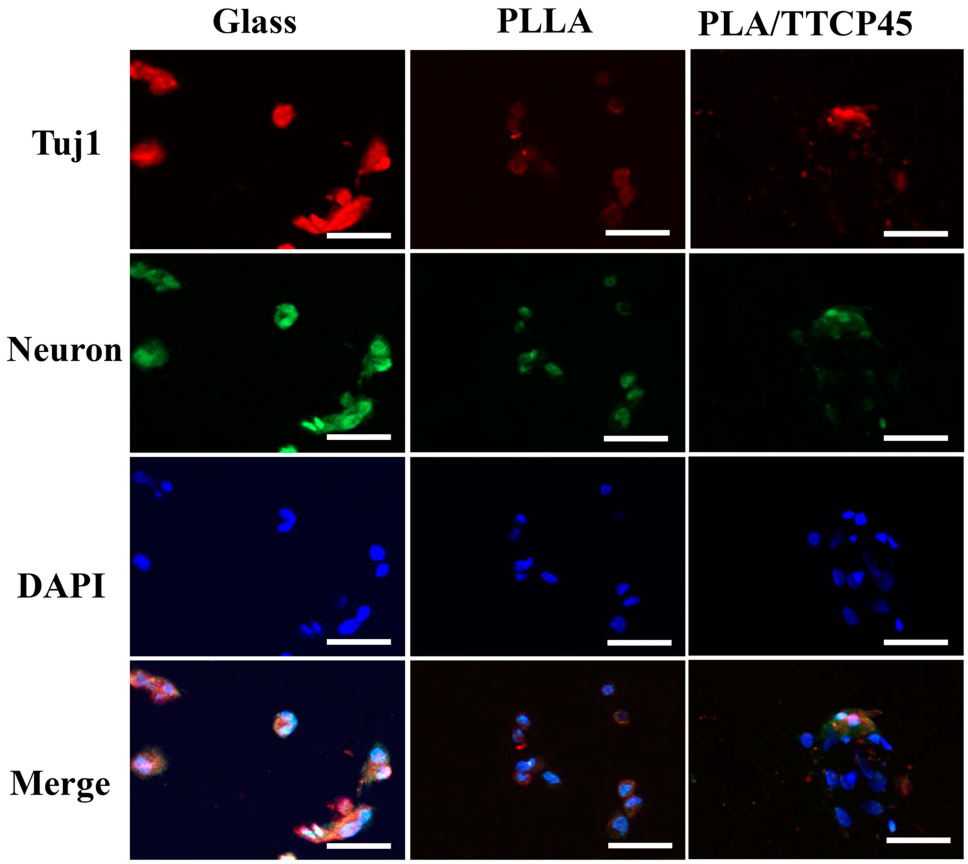

Figure 8 Differentiation of MSCs on nanofiber membranes. Immunostaining of neuron (green), tuj1 (red) and DAPI (blue) of MSCs cultured on day 9. Scale bars represent 40 μm.

TTCP45 was 47.4%. The composite nanofibers, PLA/TTCP45 and PLA/TTCP55, maintained its straight outlook after heating. The melting temperature of composite nanofiber membranes was around 222°C, higher than that of PLLA. It indicated the heat resistance of the composite nanofiber membranes. The elongation break and ultimate tensile strength of PLA/TTCP45 were 111.20% and 6.46 MPa, respectively, which were close to that of native human dura mater. In vitro cytotoxicity test showed that MSCs exhibited time-depended increase indicating the biocompatibility of composite nanofiber membranes. MSCs could differentiate into neuron-like cells on PLA/TTCP45 as on PLLA and glass, indicating the neuron compatibility of PLA/TTCP45. In a word, PLA/TTCP45 exhibited potential application to act as a dura mater substitute.

Acknowledgment

This work was financially supported by National Natural Sciences Foundation of China (31971308), National S&T Major Project (2019ZX09301-147), Sichuan Science and Technology Program (2019YFG0265), Luzhou Science and Technology Plan (2018CDLZ-10) and 1.3.5 project for disciplines of excellence, West China Hospital, Sichuan University (ZYJC18007).

Disclosure

The authors declare no conflicts of interest in this work.

References

1. Xie J, MacEwan MR, Ray WZ, Liu W, Siewe DY, Xia Y. Radially aligned, electrospun nanofibers as dural substitutes for wound closure and tissue regeneration applications. *ACS Nano*. 2010;4(9):5027–5036. doi:10.1021/nn101554u
2. Hu Y, Dan W, Xiong S, et al. Development of collagen/polydopamine complexed matrix as mechanically enhanced and highly biocompatible semi-natural tissue engineering scaffold. *Acta Biomater*. 2017;47:135–148. doi:10.1016/j.actbio.2016.10.017
3. Xu Y, Cui W, Zhang Y, et al. Hierarchical micro/nanofibrous bioscaffolds for structural tissue regeneration. *Adv Healthc Mater*. 2017;6(13):1601457. doi:10.1002/adhm.201601457
4. Gupta S, Amrutkar DV, Mataji A, et al. Evidence for CGRP re-uptake in rat dura mater encephali. *Br J Pharmacol*. 2010;161(8):1885–1898. doi:10.1111/j.1476-5381.2010.01012.x
5. Kovacs GG, Lutz MI, Ricken G, et al. Dura mater is a potential source of A beta seeds. *Acta Neuropathol*. 2016;131(6):911–923. doi:10.1007/s00401-016-1565-x

6. Wei XM, Melemedjian OK, Ahn DDU, Weinstein N, Dussor G. Dural fibroblasts play a potential role in headache pathophysiology. *Pain*. 2014;155(7):1238–1244. doi:10.1016/j.pain.2014.03.013
7. Li Q, Zhang F, Wang H, Pan T. Preparation and characterization of a novel acellular swim bladder as dura mater substitute. *Neurol Res*. 2019;41(3):242–249. doi:10.1080/01616412.2018.1550139
8. Xu C, Ma X, Chen S, Tao M, Yuan L, Jing Y. Bacterial cellulose membranes used as artificial substitutes for dural defection in rabbits. *Int J Mol Sci*. 2014;15(6):10855–10867. doi:10.3390/ijms150610855
9. Mohtaram NK, Ko J, Agbay A, et al. Development of a glial cell-derived neurotrophic factor-releasing artificial dura for neural tissue engineering applications. *J Mat Chem B*. 2015;3:7974–7985. doi:10.1039/c5tb00871a
10. Wang Y-F, Guo H-F, Ying D-J. Multilayer scaffold of electrospun PLA-PCL-collagen nanofibers as a dural substitute. *J Biomed Mater Res Part B*. 2013;101:1359–1366. doi:10.1002/jbmb.32953
11. Li Q, Mu L, Zhang F, et al. A novel fish collagen scaffold as dural substitute. *Mater Sci Eng C Mater*. 2017;80:346–351. doi:10.1016/j.msec.2017.05.102
12. Yu HC, Zhang H, Ren K, et al. Ultrathin kappa-carrageenan/chitosan hydrogel films with high toughness and antiadhesion property. *ACS Appl Mater Interfaces*. 2018;10(10):9002–9009. doi:10.1021/acsami.7b18343
13. Bohoun CA, Goto T, Morisako H, Nagahama A, Tanoue Y, Ohata K. Skull base dural repair using autologous fat as a dural substitute: an efficient technique. *World Neurosurg*. 2019;127:e896–e900. doi:10.1016/j.wneu.2019.03.293
14. Lee MW, An S, Yoon SS, Yarin AL. Advances in self-healing materials based on vascular networks with mechanical self-repair characteristics. *Adv Colloid Interface Sci*. 2018;252:21–37. doi:10.1016/j.cis.2017.12.010
15. Ghobeira R, Philips C, De Naeyer V, et al. Comparative study of the surface properties and cytocompatibility of plasma-treated poly-epsilon-caprolactone nanofibers subjected to different sterilization methods. *J Biomed Nanotechnol*. 2017;13(6):699–716. doi:10.1166/jbn.2017.2377
16. Yang HS, Zhu GL, Huang YC, Shi XT, Wang YJ. The stimulation of the differentiation of pheochromocytoma (PC12-L) cells into neuron-like cells by electrically conductive nanofibre mesh. *Appl Mater Today*. 2016;5:215–222. doi:10.1016/j.apmt.2016.09.017
17. Curvello R, Raghuwanshi VS, Garnier G. Engineering nanocellulose hydrogels for biomedical applications. *Adv Colloid Interface Sci*. 2019;267:47–61. doi:10.1016/j.cis.2019.03.002
18. Guo G, Fu S, Zhou L, et al. Preparation of curcumin loaded poly (epsilon-caprolactone)-poly(ethylene glycol)-poly(epsilon-caprolactone) nanofibers and their in vitro antitumor activity against glioma 9L cells. *Nanoscale*. 2011;3(9):3825–3832. doi:10.1039/c1nr10484e
19. Tang SY, Guo ZN, Shao JD, et al. Drawing-fabrication of multifarious nanoplasmonic platform on PLLA paper for optimized SERS performance. *J Raman Spectrosc*. 2016;47:687–691. doi:10.1002/jrs.4889
20. Xie XR, Li DS, Su CM, et al. Functionalized biomimetic composite nanofibrous scaffolds with antibacterial and hemostatic efficacy for facilitating wound healing. *J Biomed Nanotechnol*. 2019;15:1267–1279. doi:10.1166/jbn.2019.2756
21. Li P, Shang Z, Cui K, et al. Coaxial electrospinning core-shell fibers for self-healing scratch on coatings. *Chin Chem Lett*. 2019;30:157–159. doi:10.1016/j.cclet.2018.01.037
22. Han F, Zhang P, Chen T, Lin C, Wen X, Zhao P. A LbL-assembled bioactive coating modified nanofibrous membrane for rapid tendon-bone healing in ACL reconstruction. *Int J Nanomed*. 2019;14:9159–9172. doi:10.2147/ijn.s214359
23. Miszuk JM, Xu T, Yao Q, et al. Functionalization of PCL-3D electrospun nanofibrous scaffolds for improved BMP2-induced bone formation. *Appl Mater Today*. 2018;10:194–202. doi:10.1016/j.apmt.2017.12.004
24. Wang YL, Guo G, Chen HF, et al. Preparation and characterization of polylactide/poly(epsilon-caprolactone)-poly(ethylene glycol)-poly (epsilon-caprolactone) hybrid fibers for potential application in bone tissue engineering. *Int J Nanomed*. 2014;9:1991–2003. doi:10.2147/ijn.s55318
25. Augustine R, Zahid AA, Hasan A, Wang M, Webster TJ. CTGF loaded electrospun dual porous core-shell membrane for diabetic wound healing. *Int J Nanomedicine*. 2019;14:8573–8588. doi:10.2147/ijn.s224047
26. Flanagan KE, Tien LW, Elia R, Wu J, Kaplan D. Development of a sutureless dural substitute from Bombyx mori silk fibroin. *J Biomed Mater Res Part B*. 2015;103(3):485–494. doi:10.1002/jbm.b.33217
27. Shi Z, Xu T, Yuan Y, et al. A new absorbable synthetic substitute with biomimetic design for dural tissue repair. *Artif Organs*. 2016;40(4):403–413. doi:10.1111/aor.12568
28. Zwirner J, Ondruschka B, Scholze M, Schulze-Tanzil G, Hammer N. Mechanical and morphological description of human acellular dura mater as a scaffold for surgical reconstruction. *J Mech Behav Biomed Mater*. 2019;96:38–44. doi:10.1016/j.jmbbm.2019.04.035
29. Li Z, Muiruri JK, Thitsartarn W, Zhang X, Tan BH, He C. Biodegradable silica rubber core-shell nanoparticles and their stereocomplex for efficient PLA toughening. *Compos Sci Technol*. 2018;159:11–17. doi:10.1016/j.compscitech.2018.02.026
30. Meyer A, Weidner SM, Kricheldorf HR. Stereocomplexation of cyclic polylactides with each other and with linear poly(L-lactide)s. *Polym Chem*. 2019;10:6191–6199. doi:10.1039/c9py01236b
31. Muiruri JK, Liu S, Teo WS, Yeo JCC, Thitsartarn W, He C. Cavitation-crazing transition in rubber toughening of poly(lactic acid)-cellulose nanocrystal composites. *Compos Sci Technol*. 2018;168:12–19. doi:10.1016/j.compscitech.2018.08.021
32. Arias V, Odelius K, Hoglund A, Albertsson A-C. Homocomposites of polylactide (PLA) with induced interfacial stereocomplex crystallites. *ACS Sustain Chem Eng*. 2015;3(9):2220–2231. doi:10.1021/acssuschemeng.5b00498
33. Kurokawa N, Hotta A. Thermomechanical properties of highly transparent self-reinforced polylactide composites with electrospun stereocomplex polylactide nanofibers. *Polymer*. 2018;153:214–222. doi:10.1016/j.polymer.2018.08.018
34. Tsuji H, Nakano M, Hashimoto M, Takashima K, Katsura S, Mizuno A. Electrospinning of poly(lactic acid) stereocomplex nanofibers. *Biomacromolecules*. 2006;7:3316–3320. doi:10.1021/bm060786e
35. Kang Y, Chen P, Shi X, Zhang G, Wang C. Multilevel structural stereocomplex polylactic acid/collagen membranes by pattern electrospinning for tissue engineering. *Polymer*. 2018;156:250–260. doi:10.1016/j.polymer.2018.10.009
36. Kang Y, Wang C, Qiao Y, et al. Tissue-engineered trachea consisting of electrospun patterned sc-PLA/GO-g-IL fibrous membranes with antibacterial property and 3D-printed skeletons with elasticity. *Biomacromolecules*. 2019;20:1765–1776. doi:10.1021/acs.biomac.9b00160
37. Ren Y, Mei L, Gu Y, et al. Stereocomplex crystallite-based eco-friendly nanofiber membranes for removal of Cr(VI) and antibacterial effects. *ACS Sustain Chem Eng*. 2019;7(19):16072–16083. doi:10.1021/acssuschemeng.9b02828
38. Mei L, Fan RR, Li XL, et al. Nanofibers for improving the wound repair process: the combination of a grafted chitosan and an antioxidant agent. *Polym Chem*. 2017;8(10):1664–1671. doi:10.1039/c7py00038c
39. Shang YN, Wang ZY, Zhang RS, et al. A novel thermogel system of self-assembling peptides manipulated by enzymatic dephosphorylation. *Chem Commun*. 2019;55(35):5123–5126. doi:10.1039/c9cc00401g
40. Zhang X, Nakagawa R, Chan KHK, Kotaki M. Mechanical property enhancement of polylactide nanofibers through optimization of molecular weight, electrospinning conditions, and stereocomplexation. *Macromolecules*. 2012;45(13):5494–5500. doi:10.1021/ma300289z

41. Saeidlou S, Huneault MA, Li H, Park CB. Effect of nucleation and plasticization on the stereocomplex formation between enantiomeric poly(lactic acid)s. *Polymer*. 2013;54:5762–5770. doi:10.1016/j.polymer.2013.08.031
42. Na B, Zhu J, Lv RH, Ju YH, Tian RP, Chen BB. Stereocomplex formation in enantiomeric polylactides by melting recrystallization of homocrystals: crystallization kinetics and crystal morphology. *Macromolecules*. 2014;47(1):347–352. doi:10.1021/ma402405c
43. Mei L, Ren Y, Gu Y, et al. Strengthened and thermally resistant poly (lactic acid)-based composite nanofibers prepared via easy stereocomplexation with antibacterial effects. *ACS Appl Mater Interfaces*. 2018;10(49):42992–43002. doi:10.1021/acsami.8b14841
44. Tsuji H, Yamamoto S. Enhanced stereocomplex crystallization of biodegradable enantiomeric poly(lactic acid)s by repeated casting. *Macromol Mater Eng*. 2011;296:583–589. doi:10.1002/mame.201000397
45. Liu T, Huang K, Li L, et al. High performance high-density polyethylene/hydroxyapatite nanocomposites for load-bearing bone substitute: fabrication, in vitro and in vivo biocompatibility evaluation. *Compos Sci Technol*. 2019;175:100–110. doi:10.1016/j.compscitech.2019.03.012
46. Zhang D, Liu X, Wu G. Forming CNT-guided stereocomplex networks in polylactide-based nanocomposites. *Compos Sci Technol*. 2016;128:8–16. doi:10.1016/j.compscitech.2016.03.003